— J Phys Chem B —

Local THz time-domain spectroscopy of duplex DNA via fluorescence of an embedded probe

Supporting Information

André Dallmann, Matthias Pfaffe, Clemens Mügge, Rainer Mahrwald, Sergey A. Kovalenko, Nikolaus P. Ernsting*

Department of Chemistry, Humboldt University of Berlin, Germany

E-mail: nernst@chemie.hu-berlin.de.

1. Description of spectral change upon hybridisation

Different stages of the HNF absorption band are compared on a wavenumber scale in Fig. S1. By fitting a band with a lognormal function,[1] the peak position is determined fairly accurately (±10 cm^{-1}). The free chromophore is represented by the 2' -deoxyriboside of HNF in water (dRi-HNF, dashed line) with a peak at 27720 cm^{-1}. In the single strand (blue) the peak is seen at 27010 cm^{-1}, and it moves to 25820 cm^{-1} in the duplex. The HNF absorption becomes overlaid with nucleobase absorption as photon energy is increased, but the $S_1 \leftarrow S_0$ band may still be defined in the overlap region. This is done by comparison with free HNF in methanol. In that case the lowest absorption band is sufficiently separated from the higher transitions; it is also decribed by a single lognormal function. Assuming that the description holds for HNF-DNA as well, we fit the absorbance below 28700 cm^{-1} by a lognormal function and extend the latter towards higher wavenumbers $\tilde{\nu}$ (green line).

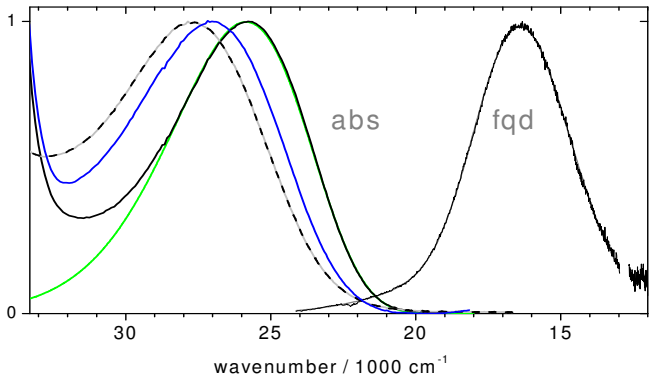

Fig. S1 Absorption spectrum and fluorescence quantum distribution of the HNF chromophore in duplex DNA (solid black lines). In single-stranded DNA (blue) the absorption band is up-shifted by 1190 cm^{-1} and for the 2´-deoxy riboside in water at 25°C (dashed) by a further 710 cm^{-1}. The $S_1 \leftarrow S_0$ absorption band in the duplex (green) was defined by comparison with unsubstituted HNF in various solvents.

The determination of the $S_1 \leftarrow S_0$ band $\varepsilon_{10}(\tilde{\nu})$ to its full extent makes the oscillator strength $\int \varepsilon_{10}(\tilde{\nu})\tilde{\nu}^{-1}d\tilde{\nu}$ available. The same oscillator strength should apply to the emission $S_1 \rightarrow S_0$ which is shown as fluorescence quantum distribution in the figure. This connection between absorption and emission band is needed when transient absorption spectra are analyzed.

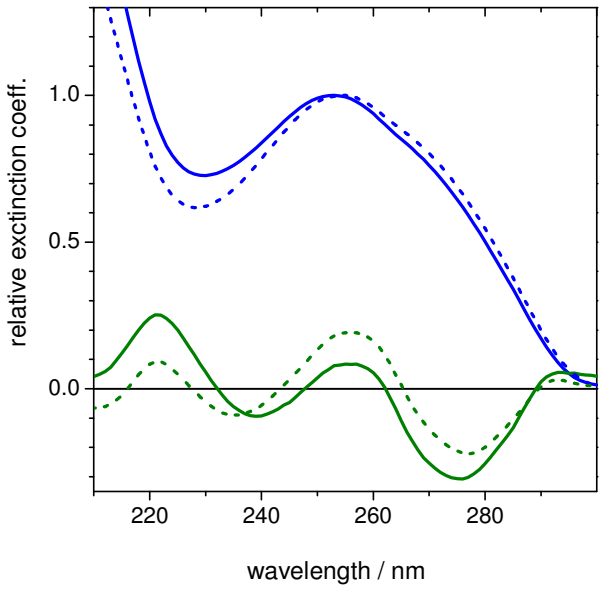

Fig. S2 Principal components of spectral change upon hybridisation of HNF-DNA (solid lines). The corresponding spectra when HNF is replaced by a GC base pair are shown with dashed lines.

How spectra change with temperature is quantified next. The UV absorption spectra are corrected for density change and then analyzed for principal components. Only two spectra, shown as solid lines in Fig. S2, are needed to describe the hyperchromism in the UV. The first is the absorption spectrum at 85°C (blue). As the duplex forms, its amplitude decreases from 1 to 0.74 as shown in Fig. 2 of the paper (blue points, right scale). In parallel the second spectral component (solid olive line in Fig. S2) increases its amplitude from 0 to 0.26 (the same amount by design) with identical behavior. A melting point of 64°C is noted for the pertinent total concentration c_T=23.5 µM of single strands. It is interesting to compare with the behavior of the HNF

absorption band, by following its peak position as temperature is lowered (red points in Fig. 2, left scale). With this measure the melting point is located 3°C lower, indicating local melting or bubble formation around the chromophore which will be examined next.

2. Simulation of melting curves with a modified zipper model

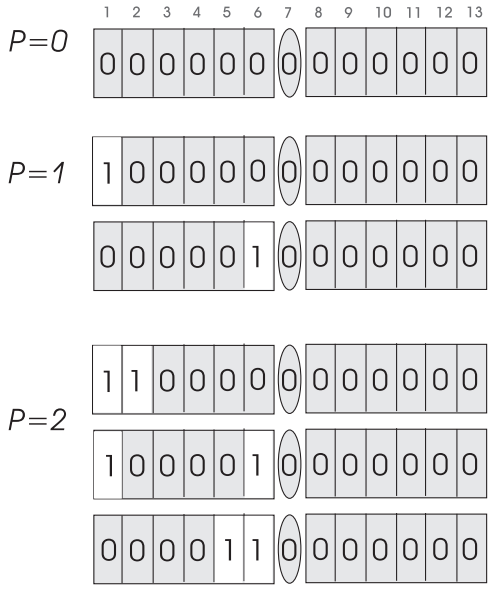

Fig. S3 Scheme of basepairs (rectangular boxes) and chromophore F (ellipse) forming duplex DNA. Gray filling indicates that a basepair is bound or that the chromophore stacked in the duplex, respectively. A number p of open sites may be distributed over the 13 positions; see text.

The calculation of the melting curves in Fig. 2 follows Ivanov *et al*[2] who allowed the formation of a central bubble. Our model is here explained so that it can be applied without further support. The basepairs and the "pair" consisting of chromophore F together with the abasic site opposite are labelled 1-13 as shown in Fig. S3. A left block is formed by basepairs 1-6, the chromophore F is in position 7, and a right block consists of basepairs 8-13. For any given temperature T the separated single strands are used for reference, *i.e.* the corresponding Gibbs energy is set to zero. The Gibbs energy G_0 of the completely bound duplex is

$$G_0 = -11g_b - g_d - g_x \qquad \text{(S1)}$$

Here $g_b > 0$ is the (reaction) Gibbs energy for breaking and unstacking a single basepair while at least one other pair is still intact, g_d is the Gibbs energy for breaking a last basepair which still holds the complementary strands together, and g_x is the Gibbs energy for unstacking the chromophore F from in between two neighboring basepairs. The temperature dependencies are formulated as

$$\begin{aligned} g_b &= h_b - Ts_b \ , \\ g_d &= h_b - Ts_d \ , \\ g_x &= h_x - Ts_x \ . \end{aligned} \qquad \text{(S2)}$$

The thermodynamic parameters to be optimized are h_b, s_b, s_d, h_x, and s_x .

In the zipper model a given number p of broken basepairs is distributed such that fraying occurs at both ends of the duplex, while pairs in between remain closed and stacked together. In the present application this condition is applied to each of the "proper" DNA blocks 1-6 and 8-13 separately, allowing the formation of a bubble around F. For example Fig. S3 shows the two possibilities when p=1 and the three possibilities when p=2 in the left block. A configuration C={$C_{(1)}$, $C_{(2)}$, …$C_{(13)}$} is indicated by $C_{(j)}$=0 (closed and stacked) or 1 (broken or unstacked) for sites j.

We proceed to calculate the configurational partition function q . For this purpose all possible configurations are first generated, but the completely open case and the case with only F stacked are subsequently deleted. Thus altogether 966 configurations are admitted. Each of them represents a distinguishable subensemble for which the Gibbs energy (relative to completely separated single strands) must be provided. We set

$$G_C = G_0 + p_{left} g_b + p_{right} g_b + f_{left} + f_{right} \qquad \text{(S3)}$$

where $p_{left} = \sum C(j)$ and $p_{rightt} = \sum C(j)$, while f_{left} and f_{right} represent the Gibbs energy for unstacking F from its nearest neigbours:

$$f_{left} = \begin{cases} 0 & \text{if } C(6) = 0 \text{ and } C(7) = 0 \\ g_x / 2 & \text{otherwise} \end{cases} \qquad \text{(S4)}$$

$$f_{right} = \begin{cases} 0 & \text{if } C(7) = 0 \text{ and } C(8) = 0 \\ g_x / 2 & \text{otherwise} \end{cases}$$

The configurational partition function q and the probability w_C of a configuration are calculated (with gas constant R)

$$q = \sum \exp(-G_C / RT), \qquad w_C = \exp(-G_C / RT)/q\,. \tag{S5}$$

Let c_T be the total molar concentration of single-stranded DNA, which is usually determined from the UV absorbance at high temperature, and assume equal concentrations for the two complementary strands. The molar concentration of the duplex is $c_{duplex} = X \cdot 0.5 \cdot c_T$ and of either free single strand $c_{ss} = (1 - X) \cdot 0.5 \cdot c_T$, where X is the degree of hybridisation, $ss_1 + ss_2 \Leftrightarrow$ duplex. Since q is the equilibrium constant one has

$$X = \frac{1 + qc_T - \sqrt{1 + 2qc_T}}{qc_T} \tag{S6}$$

Finally the observables must be calculated. These are the relative number of bound basepairs

$$B = X \cdot \sum w_C \cdot (12 - p_{left} - p_{right}) \tag{S7}$$

and the relative red-shift of the visible absorption band

$$R = X \cdot \sum w_C \cdot (r_{left} + r_{right}) \quad \text{where} \tag{S8}$$

$$r_{left} = \begin{cases} 1/2 & \text{if } C(6) = 0 \text{ and } C(7) = 0 \\ 0 & \text{otherwise} \end{cases},$$

$$r_{right} = \begin{cases} 1/2 & \text{if } C(7) = 0 \text{ and } C(8) = 0 \\ 0 & \text{otherwise} \end{cases}$$

Curves B(T) and R(T) are scaled to the observed amplitude and shift change between 25 and 85°C, respectively, and are then shown in Fig. 2. The optimal parameters are:
h_b= 39.306 kJ/mol, s_b= 113.11 J/mol K, s_d= 85.6 J/mol K,

h_x= 72.422 kJ/mol, s_x=194.3 J/mol K.

3. NMR structure determination

a) Simulated Annealing calculations

NOE peak volumes were converted to distance restraints by referencing peak classes to NOE peak volumes of known fixed distances. RDC data were acquired by determining $^1J_{(CH)}$ coupling constants (with 0.6 Hz precision) in HMQC-spectra measured with and without addition of phage Pf1 for weak alignment. C-H RDCs of T methyl groups were converted to the respective C-C RDCs using the conversion factor -0.3155. To account for different gyromagnetic ratios and bond lengths the XPLOR-NIH procedure "scale_toCH" was utilized. A total of 124 dihedral backbone restraints, 72 hydrogen bond distance restraints, 19 experimental RDC restraints and 401 (403) experimental NOE-derived distance restraints were used in calculations for the face-up (-down) orientation. Simulated Annealing calculations consisted of *(1)* 1000 steps of initial Cartesian coordinate minimization and *(2)* 50 ps of torsional angle dynamics at 20000 K, *(3)* annealing to 3000 K in 500 K steps of 500 fs duration each, and finally *(4)* annealing to 25 K in 25 K steps of 500 fs duration each. The protocol ended with 3000 steps of Cartesian Coordinate minimization. All calculations were performed with XPLOR-NIH v2.20. Parameters for the HNF residue were taken from DFT calculations performed with the program GAUSSIAN03, TZVP as basis set and the CHelpG algorithm to derive atomic charges via the Molecular Electrostatic Potential.[3] Back-calculation of the NOESY-spectra was performed with XPLOR-NIH and visualized with the program GIFA.

b) Chemical shifts

Table 1: Chemical shifts of the sugar protons in the HNF duplex relative to the HOD signal at 4.71 ppm.

Res	H1'	H2'	H2''	H3'	H4'
1	5.78	2.45	2.57	4.64	4.06
2	5.87	1.92	2.32	4.63	4.05
3	5.53	1.91	2.23	4.67	3.94
4	5.62	2.43	2.47	4.78	4.16
5	5.25	1.75	2.09	4.60	3.94
6	6.12	2.60	2.56	4.84	4.18
7	5.10	2.08	2.16	4.66	4.43
8	5.87	2.29	2.59	4.76	4.21
9	5.28	1.73	2.12	4.60	3.93
10	5.74	2.40	2.56	4.74	4.15
11	5.83	1.88	2.25	4.66	4.01
12	5.50	1.82	2.16	4.64	3.92
13	5.96	2.42	2.18	4.49	3.98
14	5.50	1.63	2.14	4.48	3.85
15	5.23	2.51	2.58	4.79	4.11
16	6.05	2.50	2.71	4.86	4.28
17	5.36	1.73	2.10	4.61	3.94
18	5.72	2.38	2.54	4.76	4.15
19	5.89	2.13	2.31	4.72	4.01
20	3.93	2.04	2.05	4.55	3.89
21	5.57	1.78	2.23	4.69	4.11
22	5.53	2.36	2.44	4.75	4.11
23	5.23	1.75	2.09	4.60	3.94
24	5.79	2.52	2.68	4.83	4.17
25	5.60	2.26	2.44	4.75	4.14
26	5.88	1.93	2.00	4.25	3.83

Table 2: Chemical shifts of the base protons in the HNF duplex relative to the HOD signal at 4.71 ppm.

Res	H1	H2	H3	H41	H42	H5	H6	H7	H8
1	-	-	-	-	-	-	-	-	7.75
2	-	-	-	8.10	6.40	5.14	7.31	-	-
3	-	-	13.74	-	-	-	7.12	1.42	-
4	12.48	-	-	-	-	-	-	-	7.67
5	-	-	-	7.99	6.18	5.21	7.15	-	-
6	-	6.88	-	-	-	-	-	-	8.14
7	5.75	-	5.78	-	-	6.82	7.23	-	7.49
8	-	7.07	-	-	-	-	-	-	7.77
9	-	-	-	7.76	6.16	4.87	6.94	-	-
10	12.51	-	-	-	-	-	-	-	7.61
11	-	-	13.54	-	-	-	7.07	1.19	-
12	-	-	-	8.41	6.81	5.50	7.29	-	-
13	-	-	-	-	-	-	-	-	7.74
14	-	-	-	7.95	6.79	5.67	7.38	-	-
15	12.73	-	-	-	-	-	-	-	7.74
16	-	7.68	-	-	-	-	-	-	8.01
17	-	-	-	7.87	6.20	5.00	6.97	-	-
18	12.38	-	-	-	-	-	-	-	7.62
19	-	-	12.99	-	-	-	7.07	1.28	-
20	-	-	-	-	-	-	-	-	-
21	-	-	12.55	-	-	-	7.07	1.29	-
22	12.32	-	-	-	-	-	-	-	7.61
23	-	-	-	8.04	6.13	5.16	7.13	-	-
24	-	7.46	-	-	-	-	-	-	7.96
25	12.71	-	-	-	-	-	-	-	7.46
26	-	-	-	7.92	6.35	5.02	7.11	-	-

c) Structures

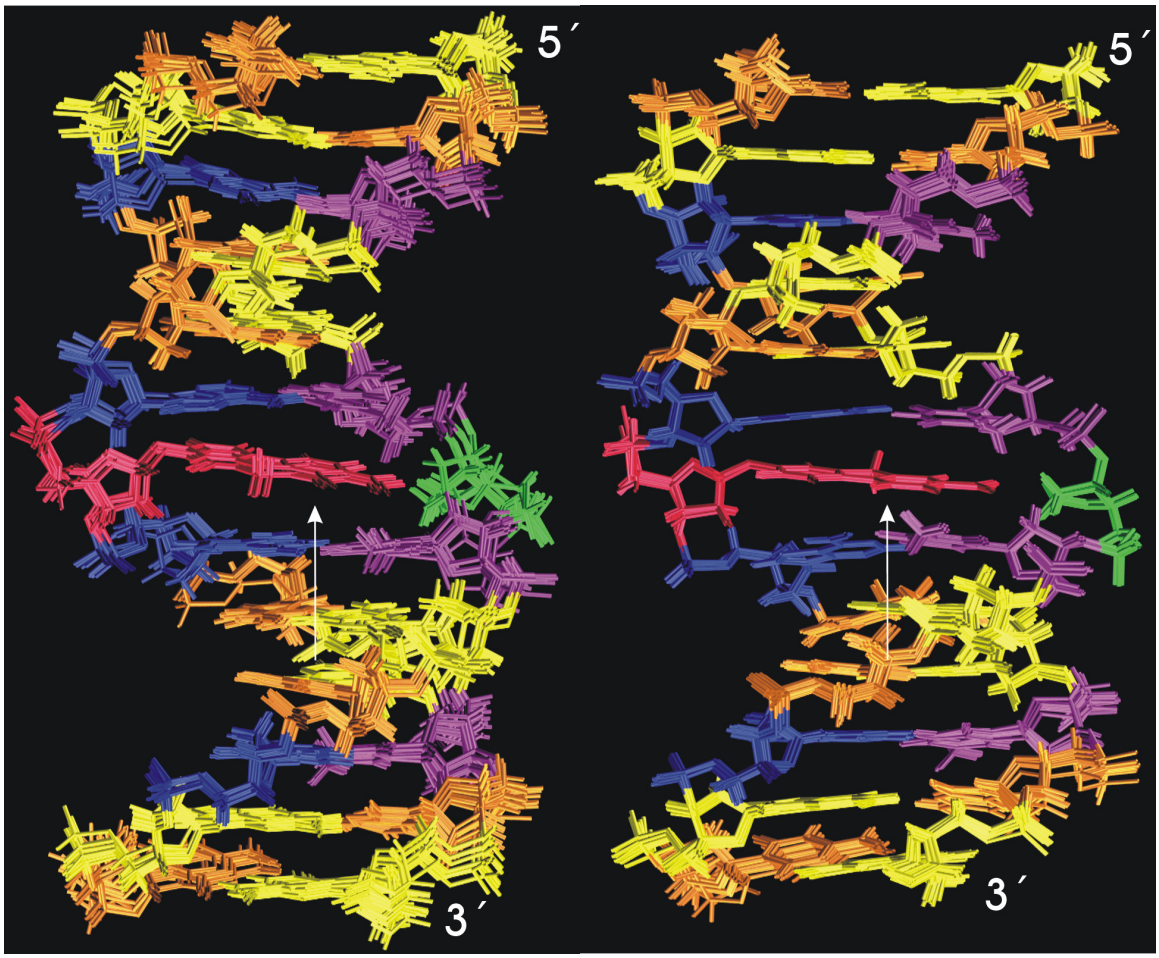

Fig. S4 Overlay of the 10 minimum-energy, violation-free structures for both orientations of the chromophore. The HNF methylene group faces up to the reader in the left panel and down in the right panel. In the latter case the position of residues is better defined compared to the former, especially around the central HNF moiety. Arrows indicate the view of Fig. S5.

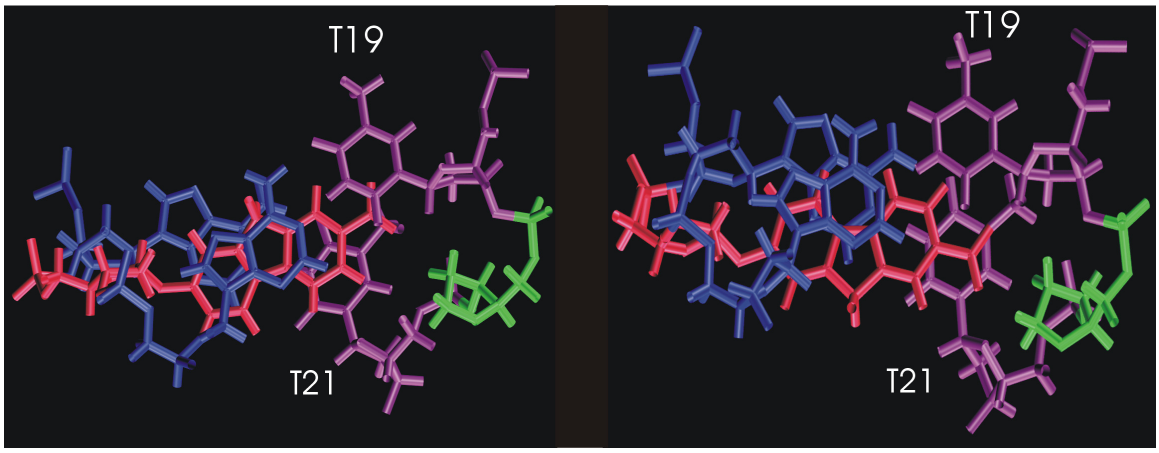

Fig. S5 Close-up view of the central region of the HNF-DNA duplex (averaged structures) with HNF face-up (left) and face-down (right). T19 has no stacking interaction with HNF, thus explaining the line-broadening of its imino proton signal. In contrast, T21 stacks perfectly with HNF.

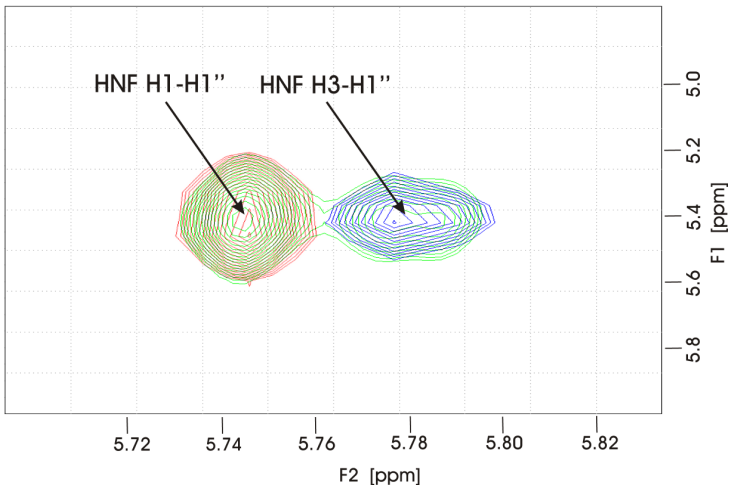

Fig. S6 Two strong experimental NOEs involving HNF can only be explained by different orientations. Overlay of the experimental (green) and back-calculated NOESY-spectra (red and blue for face-up and -down, respectively).

d) Residual Dipolar Couplings

Table 3: Residual Diploar Couplings of the HNF duplex (error: 0.6 Hz).

Res	Vector	no Pf1	with Pf1	Diff
A6	C2-H2	202.2	228.0	25.8
A8	C2-H2	201.0	223.8	22.8
A16	C2-H2	201.6	220.8	19.2
A24	C2-H2	201.0	229.8	28.8
T3	C7-H7	124.8	120.0	-4.8
T11	C7-H7	125.4	117.0	-8.4
HNF	C1'-H1"	169.2	182.4	13.2
C9	C1'-H1'	163.2	172.2	9.0
C17	C1'-H1'	161.4	166.2	4.8
T3	C6-H6	176.4	198.0	21.6
A6	C8-H8	213.6	244.2	30.6
A8	C8-H8	215.4	238.8	23.4
A16	C8-H8	213.6	234.0	20.4
A24	C8-H8	214.8	240.6	25.8
HNF	C6-H6	157.8	189.0	31.2
HNF	C8-H8	162.0	191.4	29.4
ABA	C1'-H1'	147.0	147.0	0.0
ABA	C1'-H1"	145.8	148.2	2.4

4. Analysis of femtosecond transient absorption spectra

A summary of the procedure is given first. The shape of the BL component is known from the stationary absorption spectrum. At $t = 100$ fs (the earliest delay time for which spectra were analyzed in this way) the BL and SE components are locked in amplitude through the assumption of equal oscillator strength. The other assumption is that the ESA component stays constant across the emission region ($\lambda \geq 480$ nm) with no contribution at 620 nm. There the emission is seen most purely, as indicated by the corresponding anisotropy which is maximal and constant at 0.34. The latter value is reasonably close to the theoretical value 0.4 for $S_1 \leftarrow S_0$ and $S_1 \rightarrow S_0$ transitions which are parallel. The various steps are detailed in the following.

A constant S_1 population was approximated for Fig. 8 by setting the ESA maximum =1, allowing a direct assessment of the SE band. However such normalisation is insufficient for quantitative analysis. As the prominent ESA band shifts to the blue upon solvation, it becomes located increasingly over ground-state bleach signal (*cf.* Fig.

9). For constant S_1 population one therefore expects the ESA peak to drop slightly as time proceeds, synchronous with the red-shift of the emission band. Here a self-consistent scaling procedure of transient spectra is described which allows to eliminate population decay from the data.

The procedure starts with the spectra from which the rising triplet contribution has been subtracted. In a first step, for every delay time the local minimum for $\lambda \geq 500$ nm is determined, corresponding to the peak of the emission band. From the peak wavenumbers an approximation s(t) to the spectral relaxation function is constructed ($s(0) = 1, s(\infty) = 0$). The transient spectra are then divided by

$$\mathrm{nrm} = 1 + f\left(1 - s(t)\right). \qquad \text{(S9)}$$

The correction scale factor f=0.25 is found by the requirement that the prominent ESA band has constant amplitude after full decomposition. The relative error in f is estimated below 5%; the value depends systematically on y (see below).

The model for bleached absorption and a transient stimulated emission band is explained next. Spectra are generally fitted by one or several lognormal functions[4]

$$\mathrm{lognorm}(\tilde{\nu}) \;=\; h\;\exp\left\{-\ln 2\left(\frac{\ln\left[1 + 2\,\gamma(\tilde{\nu} - \tilde{\nu}_P)/\Delta\right]}{\gamma}\right)^2\right\} \qquad \text{(S10)}$$

with parameters $\{\tilde{\nu}_P, \Delta, \gamma, h\}$ for peak wavenumber [cm^{-1}], width [cm^{-1}], asymmetry [–], and amplitude [–]. The absorption $\varepsilon_{abs}^{(HNF-DNA)}(\tilde{\nu})$ of the duplex (solid black line in Fig. S1) is described for $\tilde{\nu} \leq 32500$ cm^{-1} with the two functions given by {25836, 5677, 0.272, 0.999}, {35000, 6000, 0.0, 0.429}. The green line in Fig. S1 shows the underlying HNF absorption band $\varepsilon_{abs}^{(HNF)}(\tilde{\nu})$ which can be inferred by comparison with free HNF in methanol. Note that all absorption spectra discussed so far are relative, being normalized at the peak, and thus dimensionless. A measure for the $S_1 \leftarrow S_0$ oscillator stength is given by $\int \varepsilon_{abs}^{(HNF)}(\tilde{\nu})/\tilde{\nu}\,d\tilde{\nu} = 0.230$.

For any delay time, the band for stimulated emission $\varepsilon_{em}^{(HNF)}(\tilde{\nu})$ is now modelled as follows: (i) its lineshape or oscillator distribution $\varepsilon_{em}^{(HNF)}(\tilde{\nu})/\tilde{\nu}$ is described by a single lognormal function, and (ii) the oscillator strength is $0.230 \cdot g$ where g is allowed to decay from 1 at t=0.100 ps (the first time delay considered) to smaller values later. Condition (ii) accounts for a reduction of emissive oscillator strength over time which can be seen in the spectral evolution. The model for bleach and transient absorption is finally given by $\varepsilon_{absem}(\tilde{\nu}) = y\left[\varepsilon_{abs}^{(HNF-DNA)}(\tilde{\nu}) + \varepsilon_{em}^{(HNF)}(\tilde{\nu})\right]$. The parameters decribing the relative SE lineshape will be indicated simply by $\{\tilde{\nu}_P, \Delta, \gamma, g\}$.

The bleach amplitude is measured by the overall scale factor y. This critical parameter can in principle be determined by measurement of the absorbed pump light and its spatial distribution on the sample cell. The present experiments were performed without such controls, however, and therefore a self-consistent solution for y must be sought. By comparing the triplet-corrected, normalized (eq. S9) spectra at 0.100 ps and 24 ps we find $y = -0.72$ and $g(24ps) = 0.86$. The two values are strongly correlated, but of all possible pairs the present set leads to the most simple description of the entire spectral evolution.

The transient absorption spectrum at 24 ps marks the end of spectral change since only decay is observed afterwards (Fig. 6). At this late time the SE band is well separated from the bleach and dominant ESA bands. The pertinent values $\tilde{\nu}_P = 15856 cm^{-1}$, $\Delta = 4253 cm^{-1}, \gamma = -0.094$ for the underlying oscillator distribution are inferred from the stationary (spontaneous) fluorescence spectrum which was shown in Fig. S1. The fluorescence is dominated by contributions which are quasistationary (in effect from t≈10 ps onwards) and this is why its central portion may be used to estimate the emission lineshape at 24 ps. The parameter $g \le 0.86$ is limited from below (given y=-0.72) by the fact that excited-state absorption in the emission region must be positive. With $g = 0.86$ the ESA smoothly touches zero at 620 nm where the early anisotropy is maximal, and this was one of the reasons for making this choice. The resulting decomposition at 24 ps is shown in Fig. 9b.

Next delay times $t < 24\text{ps}$ are treated. We assume that the ESA absorption remains constant for $\lambda \geq 485\text{nm}$ where it is small anyway. The transient absorption spectra are therefore truncated to $\lambda \geq 485\text{nm}$ and the ESA spectrum determined previously (at 24 ps) is subtracted throughout. In this way the evolving SE band is estimated for every delay time. In a final step the underlying bandshape $\varepsilon_{em}^{(HNF)}(\tilde{\nu})/\tilde{\nu}$ is fitted by a lognormal function. For a second iteration cycle the relaxation function S(t) is constructed from $\tilde{\nu}_P(t)$ and then used instead of s(t) in eq. S9. The final parameters Δ, γ, $h = |y| \cdot g$ are provided in Fig. S7 ($\tilde{\nu}_P$ was already given in the main text). Extrapolation of the SE band into the bleach region enables the determination of the ESA contribution there also, which is thus complete. For example a decomposition of the spectum at 0.10 ps was demonstrated in Fig. 9a. The evolution of the peak position $\tilde{\nu}_p(t)$ of the emission lineshape was shown in Fig. 10. Multiexponential fits (red lines) resulted in the following functions:

$$\Delta(t)/\text{cm}^{-1} = 4167 - 535\exp\{-0.669t\} \pm 82 \qquad \text{(S11)}$$

$$\gamma(t) = -0.011 + 0.287\exp\{-2.54t\} - 0.141\exp\{-0.064t\} \pm 0.026$$

$$h(t) = 0.551 - 0.0475\exp\{-1.617t\} + 0.200\exp\{-0.058t\} \pm 0.009$$

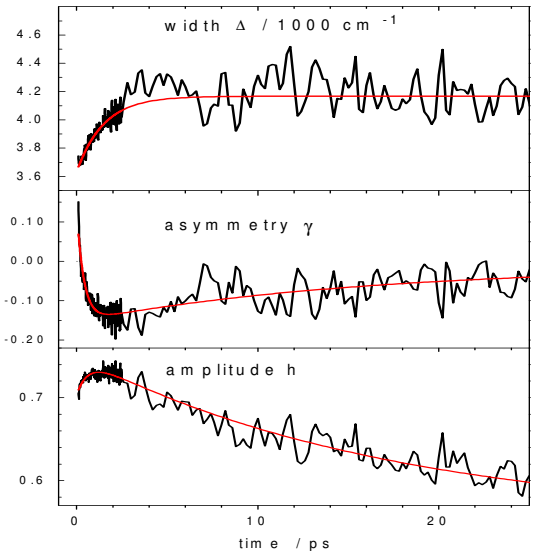

Fig. S7 Relaxation of band parameters for stimulated emission (see text).

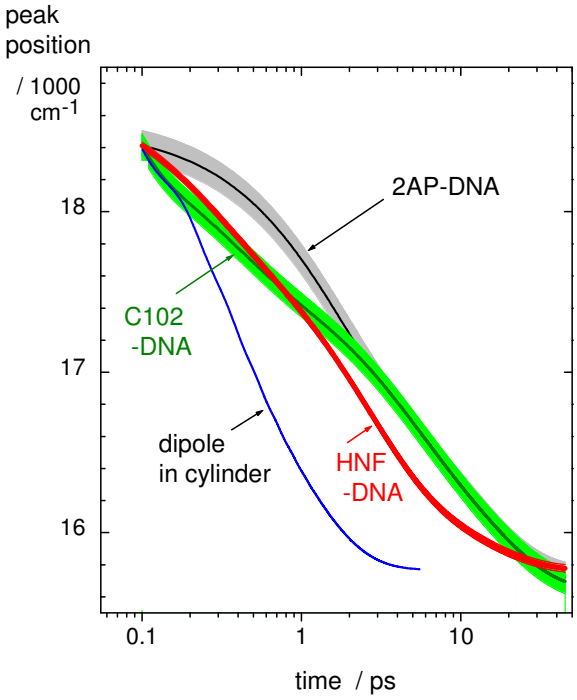

Fig. S8 Spectral relaxation curves reported for the molecular probes 2-aminopurine (2AP), coumarin 153 (C153), and hydroxy-nitro-fluorene (HNF) in dsDNA/H_2O (see text below).

Fig. S8 cites the spectral relaxation curves reported for the molecular probes 2-aminopurine (black) and coumarin 102 (green) in dsDNA. In the latter case, the data points from transient absorption measurements have been used. The curves are mapped onto the spectral relaxation curve for HNF-DNA (red) by threading them through the observed points at t=0.10 ps and 28 ps. In this way one avoids the uncertainty of peak positions at t=0 and of t_∞ . The measured shift between t=0.10 ps and 28 ps is 640, 800, and 2600 cm^{-1} for 2AP, C153, and HNF, respectively. The standard error of ± 23 cm^{-1} for the present measurement is indicated by the thickness of the red line. If the same absolute error is assumed for the other measurements, the grey and green shaded zones are obtained upon mapping.

5. Synthesis of 2-Hydroxy-7-nitro-fluorene and its nucleotide for incorporation into DNA

a) General scheme

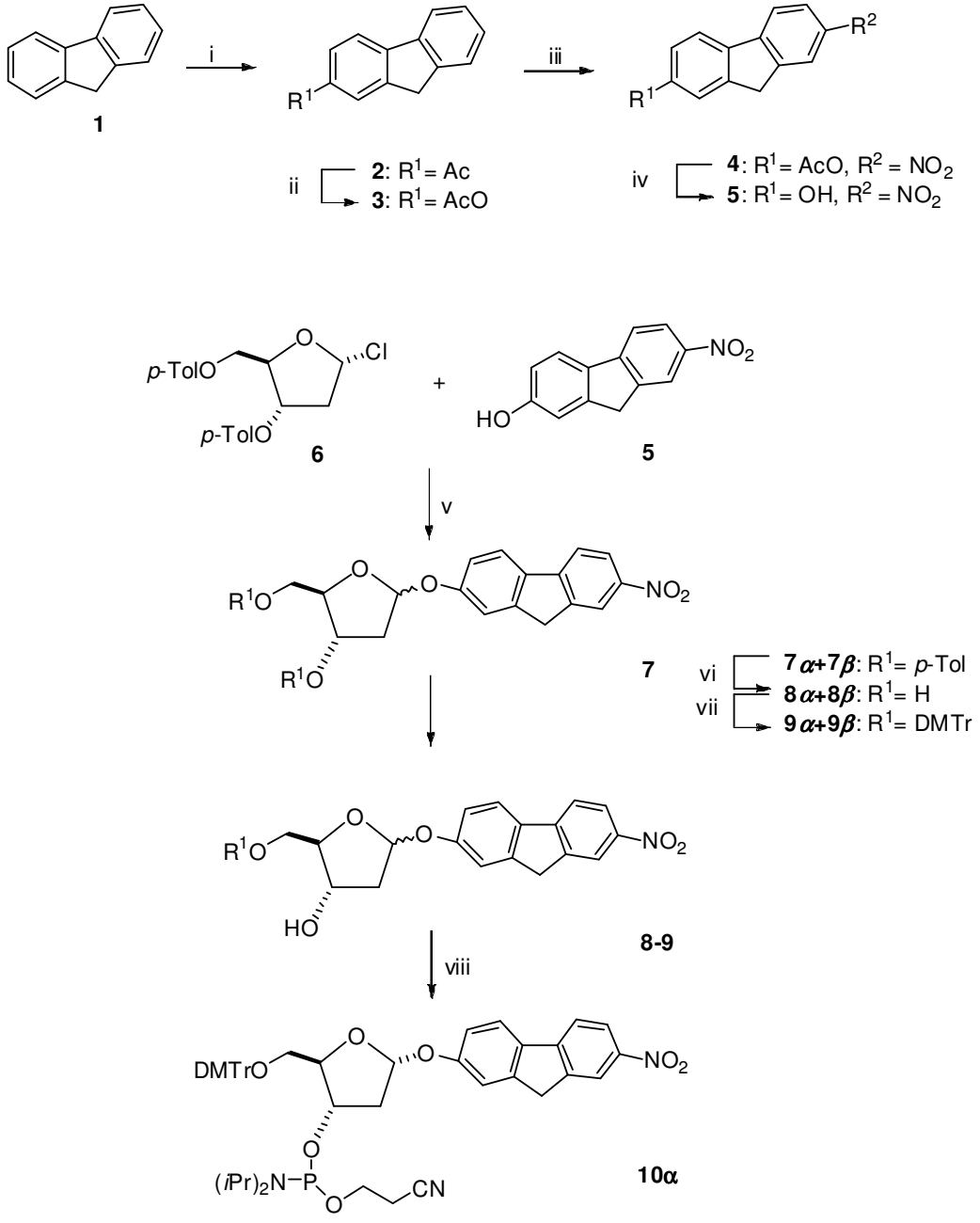

Scheme S1. Synthesis of nitrofluorenyl-deoxyriboside. *i* $MeCOCl$, $AlCl_3$; *ii* MCPBA ; *iii* HNO_3, $(MeCO)_2O$; *iv* NaOMe, MeOH; *v* molecular sieve, CH_2Cl_2; *vi* NaOMe, MeOH; *vii* DMTrCl, pyr; *viii* 2-cyanoethyl tetraisopropyl-phosphorodiamidite, 5-(benzylthio)-1*H*-tetrazole.

The synthesis of the protected nitrofluorenyl-deoxyriboside **10** was accomplished by the following reaction sequence. Readily available fluorene **1** was acetylated in the presence of $AlCl_3$.[5] Bayer-Villiger-oxidation[6] followed by nitration[7] and subsequent ester cleavage yielded aglycon **5** with 70 % yield over 4 reaction steps. The glycosidation was achieved by reaction of protected α-chloro-deoxribose **6**[8] with aglycon **5** in the presence of molecular sieve at room temperature. After deprotection and installation of dimethoxytrityl-protecting group a separation of α- and β-anomers of compound **9** could be successfully realized by column chromatography. Finally, 3'-OH was transformed into the phosphoramidite **10** by reaction of 2-cyanoethyl-tetraisopropyl-phosphordiamidite in the presence of 5-(benzylthio)-1*H*-tetrazole.

b) Experimental details

Dichloromethane and petrolether were distilled. Methanol was dried and stored over molecular sieves (4Å). All other reagents were used as obtained by the supplier without further purification. Purification of products was accomplished by flash chromatography using silica gel 60. Thin layer chromatography was carried out with Merck Silica Gel 60 F_{254} TLC plates. ^{1}H-NMR and ^{13}C-NMR spectra were recorded at 300 or 400 and 75 or 100 MHz in $CDCl_3$ (7.24; 77.0 ppm), CD_3COCD_3 (2.04; 29.3 ppm) and CD_3SOCD_3 (2.49; 39.7 ppm). Chemical shifts are given in ppm. HRMS were measured at 70 eV using an EI- or ESI-TOF spectrometer.

2-Acetylfluorene **2**

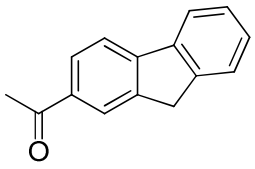

15.0 g Fluorene **1** (90.2 mmol) and 14.4 g aluminium chloride (108.3 mmol) were added to 500 ml dry dichloromethane under a nitrogen atmosphere. The red-brown suspension was cooled on an ice bath and 8.0 ml acetyl chloride (135.6 mmol) was added carefully.

After stirring overnight the reaction mixture was quenched with hydrochloric acid on ice and extracted with dichloromethane. The organic layers were separated, dried ($MgSO_4$) and evaporated i. vac. The residue was purified by column chromatography (CH_2Cl_2). 16.0 g (85 %) 2-Acetylfluorene **2** were obtained as a yellow-white solid.

^{1}H-NMR ($CDCl_3$, 300 MHz): δ= 8.12-8.09 (m, 1H, CH), 7.99-7.95 (m, 1H, CH), 7.84-7.77 (m, 2H, 2xCH), 7.58-7.53 (m, 1H, CH), 7.43-7.32 (m, 2H, 2xCH), 3.90 (s, 2H, CH_2), 2.63 (s, 3H, CH_3).
^{13}C-NMR ($CDCl_3$, 75 MHz): δ= 197.9, 146.3, 144.4, 143.2, 140.3, 135.4, 127.9, 127.6, 126.9, 125.1, 124.8, 120.8, 119.5, 36.7, 26.7.

2-Acetoxyfluorene **3**

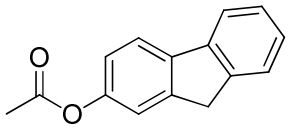

11.5 g 2-Acetylfluorene **2** (55.0 mmol) were dissolved in 250 ml chloroform and cooled under exclusion of light. 11.4 g 3-Chloroperbenzoic acid (66.0 mmol) were added carefully. The mixture was stirred for further 8 hours at 0°C and additional 5 days at room temperature. The reaction mixture was quenched with aqu. $NaHCO_3$-solution. The organic layers were separated, dried ($MgSO_4$) and evaporated i. vac. The residue was purified by column chromatography (CH_2Cl_2). 8.6 g 2-Acetoxyfluorene **3** (70 %) were obtained as a white solid.

^{1}H-NMR ($CDCl_3$, 300 MHz): δ= 7.78-7.72 (m, 2H, 2xCH), 7.55-7.50 (m, 1H, CH), 7.41--7.34 (m, 1H, CH), 7.33-7.26 (m, 2H, 2xCH), 7.12-7.07 (m, 1H, CH), 3.88 (s, 2H, CH_2), 2.33 (s, 3H, CH_3).
^{13}C-NMR ($CDCl_3$, 75 MHz): δ= 169.8, 149.6, 144.5, 143.2, 140.8, 139.5, 126.8, 126.6, 124.9, 120.3, 120.1, 119.7, 118.4, 36.9, 21.1.

HRMS: calc. for $C_{15}H_{12}O_2$: 224.08373 found: 224.08371

2-Acetoxy-7-nitrofluorene **4**

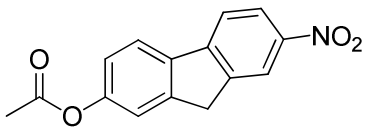

87.0 ml Acetic acid (1.5 mol) and 8.6 g 2-acetoxyfluorene **3** (38.2 mmol) were warmed to 70°C. An ice-cold solution of 1.6 ml fuming nitric acid (38.3 mmol) and 18.5 ml acetic anhydride (0.2 mol) were carefully added (reaction temperature not higher than 75°C!) and the reaction mixture was stirred overnight at room temperature. The yellow precipitate was filtrated, washed with water until neutral and dried. 9.8 g 2-Acetoxy-7-nitrofluorene **4** (95 %) were obtained as yellow solid.

^{1}H-NMR ($CDCl_3$, 300 MHz): δ= 8.38-8.32 (m, 1H, CH), 8.29-8.22 (m, 1H, CH), 7.84-7.75 (m, 2H, 2xCH), 7.35-7.29 (m, 1H, CH), 7.18-7.11 (m, 1H, CH), 3.96 (s, 2H, CH_2), 2.33 (s, 3H, CH_3).
^{13}C-NMR ($CDCl_3$, 75 MHz): δ= 169.6, 151.2, 147.2, 146.6, 146.2, 143.9, 137.2, 123.2, 122.0, 121.1, 120.4, 119.8, 118.9, 36.9, 21.1.

HRMS: calc. for $C_{15}H_{11}NO_4$: 269.06881 found: 269.06879

2-Hydroxy-7-nitrofluorene **5**

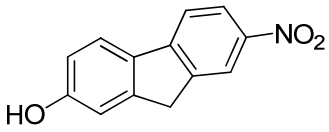

9.8 g 2-Acetoxy-7-nitrofluorene **4** (36.4 mmol) were suspended in 250 ml dry methanol. Sodium methoxide were added carefully until basic reaction. The reaction was monitored by tlc and at the end the reaction mixture was neutralized by acidic ion-exchange resin. The exchanger was filtrated, washed with methanol and the collected methanol fraction

were evaporate i. vac. 8.3 g 2-Hydroxy-7-nitrofluorene **5** (100 %) were obtained as a yellow solid.

^{1}H-NMR (CD_3COCD_3, 300 MHz): δ= 8.80 (s, 1H, OH), 8.32 (s, 1H, CH), 8.26-8.17 (m, 1H, CH), 7.91-7.78 (m, 2H, 2xCH), 7.12 (s, 1H, CH), 6.99-6.90 (m, 1H, CH), 3.96 (s, 2H, CH_2).
^{13}C-NMR (CD_3COCD_3, 75 MHz): δ= 159.4, 148.9, 148.0, 146.0, 144.0, 131.6, 123.3, 123.0, 120.4, 119.0, 115.4, 112.6, 36.8.

HRMS: calc. for $C_{13}H_9NO_3$: 227.05824 found: 227.05822

3',5'-Bis-O-(4-methylbenzoyl)-2'-deoxy-*D*-ribofuranosyl chloride **6**

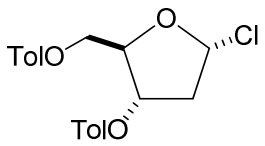

3',5'-Bis-O-(4-methylbenzoyl)-2'-deoxy-*D*-ribofuranosyl chloride **6** was prepared by the procedure of Rolland, Kotera and Lhomme[iv].

^{1}H-NMR (CD_3COCD_3, 300MHz): δ= 8.08-7.92 (m, 4H, CH_{arom}), 7.35-7.23 (m, 4H, CH_{arom}), 6.53 (d, 1H, *J*= 5 Hz, CH), 5.65-5.58 (m, 1H, CH), 4.94-4.89 (m, 1H, CH), 4.65 (dd, 1H, *J*= 4.2, 12.1 Hz, CH_2), 4.74 (dd, 1H, *J*= 3.3, 12.1 Hz, CH_2), 2.93 (ddd, 1H, *J*= 5.1, 7.4, 15.0 Hz, CH_2), 2.84-2.76 (m, 1H, CH_2), 2.47 (s, 3H, CH_3), 2.46 (s, 3H, CH_3).

7-Nitro-9*H*-fluorene-2-oyl-3',5'-bis-O-(4-methylbenzoyl)-2'-deoxy-*D*-ribofuranose **7**

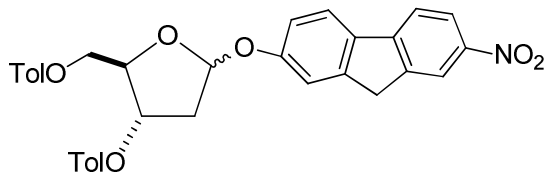

To 1.1 g 2-hydroxy-7-nitrofluorene **5** (4.7 mmol) in 100 ml dichloromethane activated molsieve (4Å) was added. A solution of 2.0 g 3',5'-bis-O-(4-methylbenzoyl)-2'-deoxy-*D*-ribofuranosyl chloride **6** (5.3 mmol) in 10 ml dichloromethane was added and the reaction mixture was stirred for further 48 h at room temperature. Molsieve was filtrated and washed with dichloromethane. The organic layers were separated, extracted with water, dried ($MgSO_4$) and evaporated i. vac. The residue was purified by column chromatography (dichloromethane/acetone - 99/1). 1.4 g **7** (52 %) were obtained as a yellow oil (ratio of $\alpha:\beta$ – 70/30).

7α:

^{1}H-NMR ($CDCl_3$, 300 MHz): δ= 8.29-8.25 (m, 1H, CH_{arom}), 8.21-8.15 (m, 1H, CH_{arom}), 8.02-7.90 (m, 3H, CH_{arom}), 7.87-7.75 (m, 3H, CH_{arom}), 7.37-7.25 (m, 4H, CH_{arom}), 7.17-7.05 (m, 2H, CH_{arom}), 6.17 (d, 1H, *J*= 4.6 Hz, CH), 5.63 (ddd, 1H, *J*= 1.6, 2.8, 7.4 Hz, CH), 4.76-4.72 (m, 1H, CH), 4.63-4.53 (m, 2H, CH_2), 3.92 (s, 2H, CH_2), 2.86 (ddd, 1H, *J*= 5.2, 7.4, 14.9 Hz, CH_2), 2.54 (dd, 1H, *J*= 0.7, 14.9 Hz, CH_2), 2.40 (s, 3H, CH_3), 2.38 (s, 3H, CH_3).

^{13}C-NMR ($CDCl_3$, 75 MHz): δ= 166.1, 166.0, 158.5, 148.3, 147.5, 146.2, 144.3, 144.2 (2xC_q), 133.5, 129.9 (2xCH), 129.8 (2xCH), 129.5 (2xCH), 129.2 (2xCH), 127.7, 127.6, 123.2, 122.7, 120.4, 119.5, 116.7, 113.5, 102.8, 83.0, 75.5, 64.5, 39.4, 37.0, 21.0 (2xCH_3).

7β:

^{1}H-NMR ($CDCl_3$, 300 MHz): δ= 8.29-8.25 (m, 1H, CH_{arom}), 8.21-8.15 (m, 1H, CH_{arom}), 8.02-7.90 (m, 3H, CH_{arom}), 7.87-7.75 (m, 3H, CH_{arom}), 7.37-7.25 (m, 4H, CH_{arom}), 7.17-7.05 (m, 2H, CH_{arom}), 6.18 (dd, 1H, *J*= 2.5, 5.4 Hz, CH), 5.75 (ddd, 1H, *J*= 3.0, 4.7, 7.3 Hz, CH), 4.72-4.66 (m, 1H, CH), 4.63-4.53 (m, 1H, CH_2), 4.45 (dd, 1H, *J*= 6.0, 11.6 Hz, CH_2), 3.84 (s, 2H, CH_2), 2.88 (ddd, 1H, *J*= 2.5, 7.3, 14.5 Hz, CH_2), 2.71 (ddd, 1H, *J*= 4.7, 5.4, 14,5 Hz), 2.40 (s, 3H, CH_3), 2.28 (s, 3H, CH_3).

^{13}C-NMR ($CDCl_3$, 75 MHz): δ= 166.0, 165.8, 158.4, 148.3, 147.4, 146.2, 144.4, 144.2, 143.9, 133.6, 129.9 (2xCH), 129.8 (2xCH), 129.5 (2xCH), 129.2 (2xCH), 127.5, 127.4, 123.1, 122.6, 120.3, 119.5, 116.6, 113.5, 103.1, 83.3, 75.1, 64.7, 39.4, 36.9, 21.0 ($2xCH_3$).

HRMS: calc. for $C_{39}H_{29}NO_8 + Na^+$: 602.1791 found: 602.1785
calc. for $C_{39}H_{29}NO_8 + NH_4^+$: 597.2237 found: 597.2231
calc. for $C_{39}H_{29}NO_8 + K^+$: 618.1530 found: 618.1521
calc. for $C_{39}H_{29}NO_8 - H^+$: 578.1820 found: 578.1820

7-Nitro-9*H*-fluorene-2-oyl-2'-deoxy-*D*-ribofuranose **8**

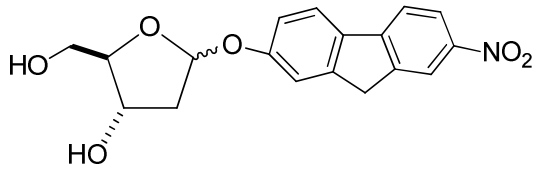

1.3 g 7-Nitro-9*H*-fluorene-2-oyl-3',5'-bis-O-(4-methylbenzoyl)-2'-deoxy-*D*-ribofuranose **7** (2.2 mmol) were suspended in dry methanol and sodium methoxide was added until basic reaction. The reaction was monitored by tlc and at the end the reaction mixture was neutralized by acidic ion-exchange resin. The exchanger was filtrated, washed with methanol and the collected methanol fraction were evaporate i. vac. The residue was purified by column chromatography (dichloromethane/methanol /petrolether - 6/3/1). 0.7 g **8** (90 %) were obtained as a yellow solid.

8*α*:

^{1}H-NMR (CD_3SOCD_3, 300 MHz): δ= 8.41-8.36 (m, 1H, CH_{arom}), 8.29-8.22 (m, 1H, CH_{arom}), 8.06-7.97 (m, 2H, $2xCH_{arom}$), 7.36-7.31 (m, 1H, CH_{arom}), 7.11-7.06 (m, 1H, CH_{arom}), 5.89 (dd, 1H, *J*= 2.1, 5.8 Hz, CH), 4.16-4.06 (m, 1H, CH), 4.03 (s, 2H, CH_2), 3.89 (ddd, 1H, *J*= 3.5, 4.9, 4.9 Hz, CH), 3.56-3.33 (m, 2H, CH_2), 2.37-2.26 (m, 1H, CH_2), 1.99 (ddd, 1H, *J*= 2.1, 4.3, 13.8 Hz, CH_2).

^{13}C-NMR (CD_3SOCD_3, 75 MHz): δ= 158.4, 148.1, 147.3, 145.5, 144.0, 132.6, 123.2, 123.0, 120.4, 119.8, 116.5, 113.2, 102.1, 86.9, 70.1, 61.3, 41.4, 36.9.

8*β*:

^{1}H-NMR (CD_3SOCD_3, 300 MHz): δ= 8.41-8.36 (m, 1H, CH_{arom}), 8.29-8.22 (m, 1H, CH_{arom}), 8.06-7.93 (m, 2H, 2xCH_{arom}), 7.34-7.29 (m, 1H, CH_{arom}), 7.06 (dd, 1H, *J*= 2.2, 8.4 Hz, CH_{arom}), 5.96 (dd, 1H, *J*= 2.7, 5.3 Hz, CH), 4.32-4.23 (m, 1H, CH), 4.03 (s, 2H, CH_2), 3.84 (ddd, 1H, *J*= 3.9, 6.0, 6.0 Hz, CH), 3.43 (dd, 1H, *J*= 6.0, 11.5 Hz, CH_2), 3.33 (dd, 1H, *J*= 5.9, 11.5 Hz, CH_2), 2.30 (ddd, 1H, *J*= 2.7, 7.1, 13.6 Hz, CH_2), 2.18 (ddd, 1H, *J*= 5.3, 5.3, 13.6 Hz, CH_2).

^{13}C-NMR (CD_3SOCD_3, 75 MHz): δ= 158.3, 148.0, 147.3, 145.5, 144.0, 132.7, 123.2, 123.0, 120.4, 119.8, 116.4, 113.3, 102.4, 88.2, 70.7, 62.9, 41.2, 36.9.

HRMS:	calc. for $C_{18}H_{17}NO_6 + Na^+$: 366.0948	found: 366.0948
	calc. for $(C_{18}H_{17}NO_6)_2 + Na^+$: 709.2004	found: 709.2004
	calc. for $C_{18}H_{16}NO_6 - H^+$: 342.0983	found: 342.0983
	calc. for $(C_{18}H_{17}NO_6)_2 - H^+$: 685.2039	found: 685.2039
	calc. for $C_{18}H_{17}NO_6 + Cl^-$: 378.0749	found: 378.0750

7-Nitro-9*H*-fluorene-2-oyl-2'-deoxy-5'-trityl-*D*-ribofuranose **9**

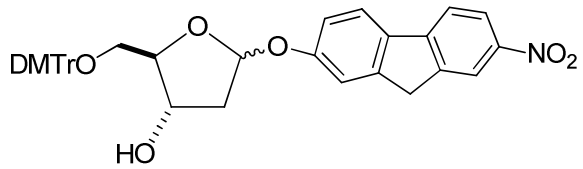

0.4 g (1.2 mmol) 7-Nitro-9*H*-fluorene-2-oyl-2'-deoxy-*D*-ribofuranose **8** were dissolved in 20.0 ml dry pyridine. 1.2 g 4,4'-Dimethoxytrityl chloride (3.5 mmol) were added and the mixture was stirred overnight. The reaction mixture was extracted with dichloromethane and aqu. NH_4Cl-solution. The organic layers were separated, dried

($MgSO_4$) and evaporated i. vac. The residue was purified by column chromatography (acetone/petrolether - 2/8). 0.5 g **9** (73 %) were obtained as a red foam.

9*α*:

^{1}H-NMR ($CDCl_3$, 400 MHz): δ= 8.36-8.33 (m, 1H, CH_{arom}), 8.28-8.23 (m, 1H, CH_{arom}), 7.77-7.72 (m, 2H, 2xCH_{arom}), 7.43-7.38 (m, 2H, CH_{arom}), 7.30-7.18 (m, 8H, CH_{arom}), 7.15-7.00 (m, 1H, CH_{arom}), 6.84-6.78 (m, 4H, CH_{arom}), 5.97 (d, 1H, *J*= 4.8 Hz, CH), 4.38-4.30 (m, 2H, 2xCH), 3.96 (s, 2H, CH_2), 3.78 (s, 6H, 2xOCH_3), 3.24 (dd, 1H, *J*= 3.8, 10.0 Hz, CH_2), 3.19 (dd, 1H, *J*= 4.9, 10.0 Hz, CH_2), 2.52 (ddd, 1H, *J*= 5.0, 6.1, 14.1 Hz, CH_2), 2.33 (dd, 1H, *J*= 0.7, 14.1 Hz, CH_2).

^{13}C-NMR ($CDCl_3$, 100MHz): δ= 158.6 (2xC_q), 157.8, 148.0, 146.9, 146.1, 144.7, 143.5, 139.5, 135.9, 135.8, 133.7, 130.1 (2xCH), 129.1, 128.1 (2xCH), 127.9 (2xCH), 126.9, 123.3, 122.3, 120.4, 119.1, 116.7, 113.5, 113.2 (5xCH), 103.5, 87.5, 73.5, 63.8, 55.2, 41.5, 37.0.

9*β*:

^{1}H-NMR ($CDCl_3$, 300 MHz): δ= 8.35-8.30 (m, 1H, CH_{arom}), 8.28-8.21 (m, 1H, CH_{arom}), 7.76-7.68 (m, 2H, CH_{arom}), 7.42-7.34 (m, 2H, CH_{arom}), 7.32-7.10 (m, 8H, CH_{arom}), 7.08-7.03 (m, 1H, CH_{arom}), 6.71-6.61 (m, 4H, CH_{arom}), 5.95 (dd, 1H, *J*= 1.7, 5.3 Hz, CH), 4.64-4.55 (m, 1H, CH), 4.14-4.05 (m, 1H, CH), 3.91 (s, 2H, CH_2), 3.67 (s, 3H, OCH_3), 3.66 (s, 3H, OCH_3), 3.28-3.15 (m, 2H, CH_2), 2.54 (ddd, 1H, *J*=1.7, 6.8, 13.1 Hz, CH_2), 2.35-2.26 (m, 1H, CH_2).

^{13}C-NMR ($CDCl_3$, 75 MHz): δ= 158.5, 158.4, 158.3, 148.1, 146.8, 145.9, 144.8, 144.7, 143.4, 135.9, 135.8, 133.1, 130.0, 129.9, 129.0, 128.1 (2xCH), 127.7 (2xCH), 126.7, 123.3, 122.1, 120.3, 118.9, 116.3, 113.1, 113.0 (5xCH), 102.2, 86.0, 72.3, 64.5, 55.1, 41.4, 36.9.

HRMS: calc. for $C_{39}H_{35}NO_8 + Na^+$: 668.2260 found: 668.2255
calc. for $C_{39}H_{35}NO_8 + NH_4^+$: 663.2706 found: 663.2701

7-Nitro-9*H*-fluoren-2-oyl-2'-deoxy-5'-trityl-□-*D*-ribofuranose phosphoramidite **10**

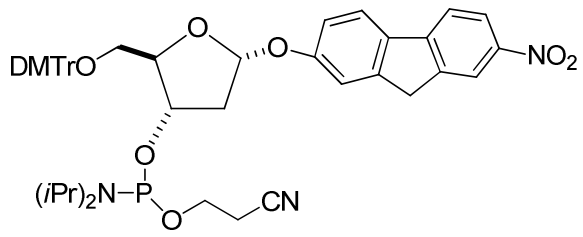

272 mg **9** 7-Nitro-9*H*-fluorene-2-oyl-2'-deoxy-5'-trityl-*D*-ribofuranose (0.4 mmol) were dissolved in dry acetonitrile. Catalytic amounts of 5-(benzylthio)-1*H*-tetrazole and 0.20 ml 2-cyanoethyl tetraisopropylphosphorodiamidite (0.6 mmol) were added. The reaction mixture was stirred for 1 hour at room temperature. The solvent was removed i. vac. and the remaining residue was purified by column chromatography (acetone/hexane - 3/7, containing 5 % triethylamine). 280 mg (79 %) **10** were obtained as a yellow oil.

Mass spectrometry (LTQ-FT) characterization of the 13mer duplex by detecting the single-strands:

Sequence	charge	calculated	found
5'-GCTGCAFACGTCG-3'	8x negative + Na^+	508.080	508.078
	7x negative + Na^+	580.807	580.803
3'-CGACGT_TGCAGC-5'	8x negative + Na^+	479.950	479.947
	7x negative + 2 Na^+	551.798	551.795

References

[1] Karunakaran, V.; Pfaffe, M.; Ioffe, I.; Senyushkina, T.; Kovalenko, S. A.; Mahrwald, R.; Fartzdinov, V.; Sklenar, H.; Ernsting, N. P.; *J. Phys. Chem. A* **2008**, *112*, 4294.

[2] Ivanov, V.; Zeng, Y. Zocchi, G.; Phys. Rev. E, **2004**, *70*, 051907

[3] Breneman, C. M.; Wiberg, K. B.; *J. Comput. Chem.* **1990**, *11***,** 361.

[4] D. B. Siano and D. E. Metzler, *J. Chem. Phys*. 1969, **51**, 1856.

[5] Rieveschl Jr., G.; Ray, F. E. *Chem. Rev.* **1938**, *23*, 287-389.

[6] Jones Jr., D. W.; Albrecht, W. L.; Palopoli, F. P. *J. Org. Chem.* **1977**, *42*, 4144-4146.

[7] (a) Bryant, H.; Sawicki, E. *J. Org. Chem.* **1956**, *21*, 1322-1324; (b) Dahlgard, M. *J. Org. Chem.* **1960**, *25*, 469-470.

[8] Rolland, V.; Kotera, M.; Lhomme, J. *Synth. Comm.* **1997**, *27*, 3505-3511.